ACS OMEGA

http://pubs.acs.org/journal/acsodf

Article

Layered Double Hydroxide-Loaded miR-30a for the Treatment of Breast Cancer In Vitro and In Vivo

Shiwen Zhang,[#] Siyan Pang,[#] Wenhao Pei,[#] Haitao Zhu, Yingxiang Shi, Ziyang Liu, Lingyu Mao, Xiuru Shi, Shuang Tao, Chenchen Geng, Sulian Chen, Linnan Yang, Changjie Chen,* Qingling Yang,* and Wenrui Wang*

Cite This: *ACS Omega* 2023, 8, 18435−18448

Read Online

ACCESS | Metrics & More | Article Recommendations

ABSTRACT: MicroRNAs (miRNAs) play an essential role in cancer therapy, but the disadvantages of its poor inherent stability, rapid clearance, and low delivery efficiency affect the therapeutic efficiency. Loading miRNAs by nanoformulations can improve their bioavailability and enhance therapeutic efficiency, which is an effective miRNA delivery strategy. In this study, we synthesized layered double hydroxides (LDH), which are widely used as carriers of drugs or genes due to the characteristics of good biocompatibility, high loading capacity, and pH sensitivity. We loaded the suppressor oncogene miR-30a on LDH nanomaterials (LDH@miR-30a) and determined the mass ratio of miRNA binding to LDH by agarose gel electrophoresis. LDH@miR-30a was able to escape the lysosomal pathway and was successfully phagocytosed by breast cancer SKBR3 cells and remained detectable in the cells after 24 h of co-incubation. In vitro experiments showed that LDH@miR-30a-treated SKBR3 cells showed decreased proliferation and cell cycle arrest in the G0/G1 phase and LDH@miR-30a was able to regulate the epithelial−mesenchymal transition (EMT) process and inhibit cell migration and invasion by targeting SNAI1. Meanwhile, in vivo experiments showed that nude mice treated with LDH@miR-30a showed a significant reduction in their solid tumors and no significant impairment of vital organs was observed. In conclusion, LDH@miR-30a is an effective drug delivery system for the treatment of breast cancer.

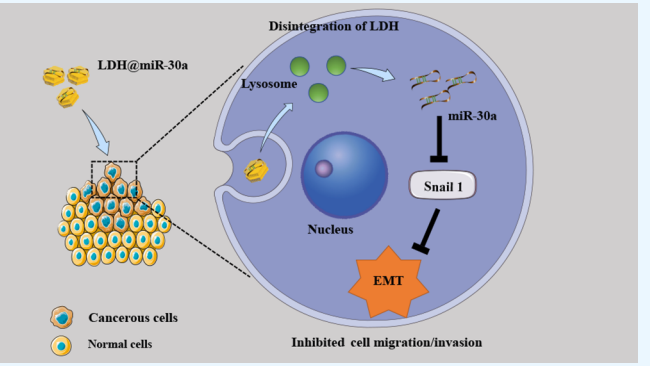

1. INTRODUCTION

Breast cancer (BC) ranks as the fifth leading cause of death from cancer overall, is the most frequent cause of cancer death in women in less-developed regions, and is the second cause of cancer death in developed countries after lung cancer.[1,2] The 2013 St. Gallen International Breast Cancer Conference issued a new definition of BC molecular subtypes: luminal A, luminal B, human epidermal growth factor receptor 2 (HER2), basal-like triple-negative breast cancer (TNBC), and other special subtypes.[3] HER2-enriched tumors are characterized by overexpression of the Erb-B2 oncogene and show low levels of ER expression.[4] Between 12 and 20% of all BCs overexpress the HER2 protein and/or have HER2 gene amplification, which results in aggressive tumor growth and poor clinical outcome.[5] This BC subtype poses major clinical challenges due to the lack of specific diagnostic/prognostic biomarkers and the failure of standard therapy to provide a targeted effect.[6] Numerous efforts have been strived to find better diagnostic and therapeutic tools for patients with BC.[7] MiRNAs have been shown to have the potential to be considered as new biomarkers in cancer diagnosis, prognosis, and response to BC therapy.

MicroRNAs (miRNAs) are small non-coding RNA molecules that trigger post-transcriptional silencing and suppress gene expression by binding to the 3′-untranslated region of target messenger RNAs.[8] Overexpressed miRNAs in tumor act as oncogenes to promote tumor development, while low-expressed miRNAs act as cancer suppressor genes to suppress tumor development.[9] As a tumor marker, miR-30a is commonly expressed in various malignant diseases and plays a key regulatory role in tumorigenesis and progression. miR-30a can play a crucial role in cancer development, including proliferation, invasion, and migration, by acting on multiple signaling

Received: December 9, 2022
Accepted: April 28, 2023
Published: May 15, 2023

pathways to regulate downstream target genes.[10,11] For example, gene set enrichment analysis (GSEA) revealed that low miR-30a expression levels in The Cancer Genome Atlas (TCGA) cohort were associated with gene enrichment in epithelial−mesenchymal transition (EMT).[12] Moreover, it has been demonstrated that miR-30a could target EMT-related molecules to inhibit tumor cell migration and invasion in BC and other solid cancers.[13−16] However, free miRNA is unstable under physiological conditions and has low cellular uptake, so therapeutic effects require a safe, non-toxic, and efficient carrier system.[17,18]

As an inorganic nanomaterial, layered double hydroxides (LDHs) are ideal drug and gene delivery carriers due to their good biocompatibility, high loading capacity, and efficient cellular uptake.[19] Previous studies have demonstrated the feasibility of LDH-loaded siRNA/miRNA as therapeutic gene drugs,[20] such as for Parkinson's disease protective treatment,[21] combined cancer co-immunotherapy,[22] or using LDH to co-deliver small interfering RNA (siRNA) and fluorouracil (5-Fu).[23]

In this study, we developed a gene-drug therapy system, LDH@miR-30a, which used LDH nanomaterials as the vector to deliver miR-30a for tumor treatment. LDH@miR-30a could escape from the lysosomal pathway, which could effectively be taken up by cells and exert cancer-suppressive effects in vitro and in vivo. These results provided a strategy for the application of nanotechnology in the clinical treatment of BC.

2. MATERIALS AND METHODS

2.1. Materials and Reagents. $MgCl_2{\cdot}6H_2O$, $AlCl_3{\cdot}9H_2O$, and NaOH were obtained from Sinopharm Chemical Reagent Co, Ltd. (Shanghai, China). Cell Counting Kit-8 (CCK8) and GelRed nucleic acid dye were purchased from Biomiky (Hefei, China). Tris−acetate−EDTA (TAE) buffer, Crystal violet solution, radioimmunoprecipitation assay (RIPA), phenylmethanesulfonyl fluoride (PMSF), BCA Protein Assay Kit, and penicillin−streptomycin were obtained from Beyotime Biotechnology (Shanghai, China). 4′,6-Diamidino-2-phenylindole (DAPI) and acridine orange (AO) staining solution were obtained from Solarbio (Beijing, China). LysoTracker Green, propidium iodide (PI), and RnaseA staining solutions were purchased from KeyGen (Nanjing, China). Matrigel gel was procured from Corning (Michigan, USA). Hematoxylin and eosin repair solution, Triton X-100, and TdT-mediated nick end labeling (TUNEL) assay kit were obtained from Servicebio (Wuhan, China). Tween 20 was obtained from Macklin (Shanghai, China). TRIzol reagent was purchased from Thermo Fisher Scientific (Massachusetts, USA). All-in-One miRNA qRT-PCR Detection Kit 2.0 and All-in-One qRT-PCR Mix were obtained from GeneCopoeia (Maryland, USA). DMEM medium, DMEM/F12 medium, and horse serum were purchased from Procell (Wuhan, China). Fetal bovine serum (FBS) was procured from Thermo Fisher Scientific (Massachusetts, USA). The primary antibodies used in the experiments including N-cadherin (1:1000, cat. no.: A19083) E-cadherin (1:1000, cat. no.: A3044), vimentin (1:1000, cat. no.: A19607), SNAI1 (1:1000, cat. no.: A5243), β-actin (1:10,000, cat. no.: AC026), and GAPDH (1:5000, cat. no.: AC001) were purchased from ABclonal (Wuhan, China). Horseradish peroxidase (HRP)-labeled goat anti-rabbit antibody (1:6000, cat. no. S0001) was purchased from Affinity Biosciences (Nanjing, China). Polyvinylidene fluoride (PVDF) membranes and chemiluminescent HRP substrate were purchased from Millipore (Missouri, USA).

These HPLC-purified RNA sequences are listed below:

miR-30a-5p sense: 5′-UGUAAACAUCCUCGACUGGAAG-3′,

antisense: 5′-UCCAGUCGAGGAUGUUUACAUU-3′.

Negative control (NC) sense: 5′-UUCUCCGAACGUGUCACGUTT-3′.

antisense: 5′-ACGUGACACGUUCGGAGAATT-3′.

These relevant purified primer sequences for SNAI1 (target protein) and β-actin (internal reference protein) are listed below:

SNAI1 forward primer: 5′-CCTCGCTGCCAATGCTCATCTG-3′.

SNAI1 reverse primer: 5′-CTCTGCCACCCTGGGACTCTC-3′.

β-actin forward primer: 5′-CCTGGCACCCAGCACAAT-3′.

β-actin reverse primer: 5′-GGGCCGGACTCGTCATAC-3′.

2.2. Cell Lines and Animals. The HER2-positive BC cell line SKBR3 and the normal mammalian cell MCF-10A were obtained from the Shanghai Institute of Biochemistry and Cell Biology, Chinese Academy of Sciences. All of the cell lines used in experiments were cultured at 37 °C in a 5% CO_2-humidified atmosphere. SKBR3 cells were maintained in DMEM with 10% FBS. MCF-10A cells were maintained in DMEM/F12 with 5% horse serum. All of the media used in experiments were supplemented with 100 μg/mL of streptomycin, 100 U/mL of penicillin.

Female Balb/c nude mice (4−5 weeks old) were purchased from Changzhou Cavins Laboratory Animal Co., Ltd. (license number: SCXK SU 2021-0013), and hosted in an SPF room of the animal house in Bengbu Medical College. All experiments were performed in accordance with the China Public Health Service Guide for the Care and Use of Laboratory Animals. Experiments involving mice and protocols were approved by the Institutional Animal Care and Use Committee of Bengbu Medical college.

2.3. Synthesis of LDH, LDH@miR-30a, and LDH@miR-30a-Cy3 NPs. The chemical synthesis of Mg-Al LDH nanoparticles was performed by co-precipitation-hydrothermal method according to a previous report. Briefly, 40 mL of NaOH solution (0.16 M) was stirred vigorously at 300 rpm at 37 °C under a nitrogen atmosphere, and after 5 min, 10 mL of mixed solution with a 3:1 molar ratio of Mg^{2+} to Al^{3+} was quickly added to make the final pH close to about 10. Next, the products were washed with decarbonated water and then aged at 100 °C for 16 h. Finally, the precipitate was separated by centrifugation at 12,000 rpm at 4 °C for 1 h, transferred to an enzyme-free Eppendorf (EP) tube, and stored at 4 °C.

Briefly, miR-30a was first dissolved in RNase-free water. Then, LDH@miR nanoparticles and LDH@NC (negative control miRNA) were prepared by shaking the mixed solution of LDH and miR-30a (LDH: miR-30a = 10:1, w/w) at 500 rpm at room temperature for 1 h. LDH@miR-30a-Cy3 was obtained by the same method, but it must be light protected to avoid fluorescence quenching of Cy3.

2.4. Characterization. X-ray diffraction (XRD) patterns of lyophilized samples were recorded using a Tensor 27 spectrometer (Bruker, Germany) and a D8 ADVANCE instrument (Bruker, Germany). The hydrodynamic particle size and the zeta potential of NPs was performed by a particle size analyzer (Zetasizer, Malvern, UK) at 25 °C. The transmission electron microscopy (TEM) images were acquired

https://doi.org/10.1021/acsomega.2c07866
ACS Omega 2023, 8, 18435−18448

on HT7700 TEM (Hitachi, Japan) at an acceleration voltage of 80 kV.

2.5. Gel Retardation Assay. The miRNA loading capacity in LDH nanoparticles was evaluated by gel retardation. LDH@miR-30a composites with different LDH to miR-30a mass ratios were prepared at a mass ratio of miRNA:LDH = 1:40, 1:20, 1:10, 1:5, and 1:1.25. The mass of miR-30a remained constant at 0.4 μg. The naked miR-30a was used as a control. For the loading ratio assay, different samples were loaded on 1% agarose gel in TAE buffer containing GelRed and subjected to electrophoresis at 110 V for 20 min. The results were visualized using a ChemiDoc XRS$^+$ system (Bio-Rad, USA).

2.6. Bioinformatic Analysis. Survival analysis was performed using the KM Plotter online analysis tool. The KM Plotter online tool was accessed, and TCGA data were selected to check the relationship between miR-30a expression and overall survival of BC patients (531 high- and 531 low-expression cases). Overall survival rates were estimated by calculating the log-rank p-value, hazard ratios (HR), and the 95% interval, and the difference was considered statistically significant at $p < 0.05$.

The difference in miR-30a expression in normal breast tissue versus BC in TCGA database was analyzed by the UALCAN online analysis tool, including 76 normal versus and 749 BCs, with the same analysis of miR-30a expression in major subclasses of BC, including 76 normal, 370 luminal, 25 HER2-positive, and 81 TNBC. The presence of complementary sites between miR-30a and the 3′-untranslated region (3′-UTR) of SNAI1 was predicted using the TargetScan online database.

2.7. Cellular Uptake and Cellular Location. For cellular uptake, LDH@miR-30a-Cy3 was used to track nanoparticles. SKBR3 cells were seeded in 35 mm glass-bottom cell culture dishes (Sorfa, Zhejiang, China) at the density of 1×10^4 cells/dish for 24 h, and the culture medium was replaced by 1 mL of medium containing 100 nM miR-30a-Cy3/LDH@miR-30a-Cy3. The mass ratio of LDH to miR-30a-Cy3 was 1:10. The cells were incubated at 37 °C for 4 and 24 h in the dark, respectively. The medium in the dish was removed, and the cells were washed three times with phosphate-buffed saline (PBS) buffer to eliminate excess particles. 400 μL of 4% paraformaldehyde (diluted with PBS) was added to fix the cell morphology at room temperature, and the cells were washed with PBS. The cell nuclei were stained with DAPI for 10 min, followed by washing with PBS three times. DAPI (Ex = 405 nm, Em = 461 nm) and Cy3 fluorescence (Ex = 543 nm, Em = 567 nm) were observed and imaged with a confocal laser microscope (CLSM, FV1200MPE, Olympus, Japan). To determine the cellular location of LDH@miR-30a, SKBR3 cells were seeded in a glass-bottom culture dish (10^4 cells/dish) and maintained in medium at 37 °C for 12 h. Then, cells were incubated with free miR-30a-Cy3/LDH@miR-30a-Cy3 for 3 h and washed twice with cold PBS to remove the surface-adhered NPs followed by staining with LysoTracker green (Ex: 443 nm, Em: 505 nm) to label endo-/lysosomes and DAPI for the nucleus, and then cellular localization was recorded under the inverted fluorescence microscope (Axio Observer Z1, Zeiss, Germany).

SKBR3 cells (1×10^4 cells) were seeded into 35 mm glass-bottomed microscope dishes and incubated for 12 h to allow the cells to attach onto the glass bottom. Then, 2 μg/mL of LDH was added to microscope dishes. After incubation for 4 h, the cells were stained with 400 μL of AO staining solution (10 μg/mL) for 15 min. The next protocols were the same as intracellular uptake. The photos were observed and imaged by using the green (Em = 488 nm, Ex = 520 nm) and red (Em = 543 nm, Ex = 603 nm) fluorescence channels of the laser confocal microscope (FV-1200MPE, Olympus, Japan).

2.8. Cell Viability Assay. SKBR3 cells were seeded into 96-well plates at a density of 5×10^3 cells per well in DMEM culture medium for 24 h. After that, the culture medium was changed with complete medium containing different concentrations of LDH, free miR-30a, and LDH@miR-30a (0, 25 nM, 50 nM, 100 nM, based on miR-30a concentration, diluted with complete medium), respectively. After 24 or 48 h of incubation, the liquid was removed by washing with PBS. Finally, 10 μL of the CCK-8 reagent was added into each well and OD at 450 nm was measured using a multifunction microplate reader (Multiskan GO, Thermo, USA) after incubation for 2 h at 37 °C. Samples were protected from light during the assays.

2.9. Cell Cycle. SKBR3 cells were seeded into six-well plates at a density of 10^5/well for overnight and then treated with free miR-30a, LDH@NC, and LDH@miR-30a (100 nM, based on miR-30a concentration) for 48 h. Cells were washed with cold PBS and harvested with 0.25% trypsin (without EDTA, diluted with D-Hank's solution). The cells were fixed in 75% ice-cold ethanol and stored at −20 °C overnight. Cells were then washed with PBS and then centrifuged at 3000 rpm for 5 min. Then, propidium iodide (PI)-RnaseA staining solution (5 μg/mL PI in PBS, and 0.5 μg/mL RNase A) was added and incubated for 30 min at 37 °C in the dark. The cell cycle distribution was then evaluated using FACS (CytoFLEX, Beckman, USA) based on the cellular DNA content.

2.10. Cell Migration and Invasion Assays. SKBR3 cells were seeded in six-well plates and cultured until fusion. Individual wounds were generated using a 10 μL sterile pipette tip to slice through the fused monolayer of cells. Cells were washed twice with PBS and then incubated with DMEM (1% FBS) containing LDH@NC, free miR-30a, or LDH@miR-30a (100 nM/2 mL, based on miR-30a concentration, diluted with complete medium). Images were recorded at 0, 24, and 48 h with an inverted microscope (CKX31, Olympus, Japan) at 40× magnification, respectively.

Invasion assays were performed on transfected SKBR3 cells using Transwell cell culture dishes (Corning, USA). SKBR3 cells (1×10^5) were seeded into six-well plates and cultured in complete DMEM medium. The cultured cells were subsequently treated with LDH, miR-30a, or LDH@miR-30a (100 nM, based on miR-30a concentration, diluted with complete medium), respectively. After 24 h of incubation, the cells were trypsinized and suspended in medium without serum. Subsequently, 1×10^4 cells were seeded in the upper chambers in 200 μL of serum-free medium and 700 μL of complete medium containing 10% FBS was added to the lower Transwell chambers. After 24 h, the nonmigrated cells in the top chamber were removed with a cotton swab. The migrated cells were fixed in 4% paraformaldehyde for 20 min and stained with 0.1% crystal violet solution for 10 min at room temperature. The images were taken by an inverted microscope (CKX31, Olympus, Japan) at 100× magnification, respectively.

2.11. RNA Extraction and Quantitative Real-Time PCR (qRT-PCR). SKBR3 cells were inoculated in six-well plates at a density of 10^5/well for 12 h and then treated with free miR-30a, LDH@NC, or LDH@miR-30a (100 nM/2 mL, based on miR-30a concentration, diluted with complete medium) for 48 h. Cells were collected after digestion with 0.25% trypsin and washed with PBS. Total RNA was extracted using TRIzol reagent. A certain volume of RNase-free H_2O was added to

https://doi.org/10.1021/acsomega.2c07866
ACS Omega 2023, 8, 18435−18448

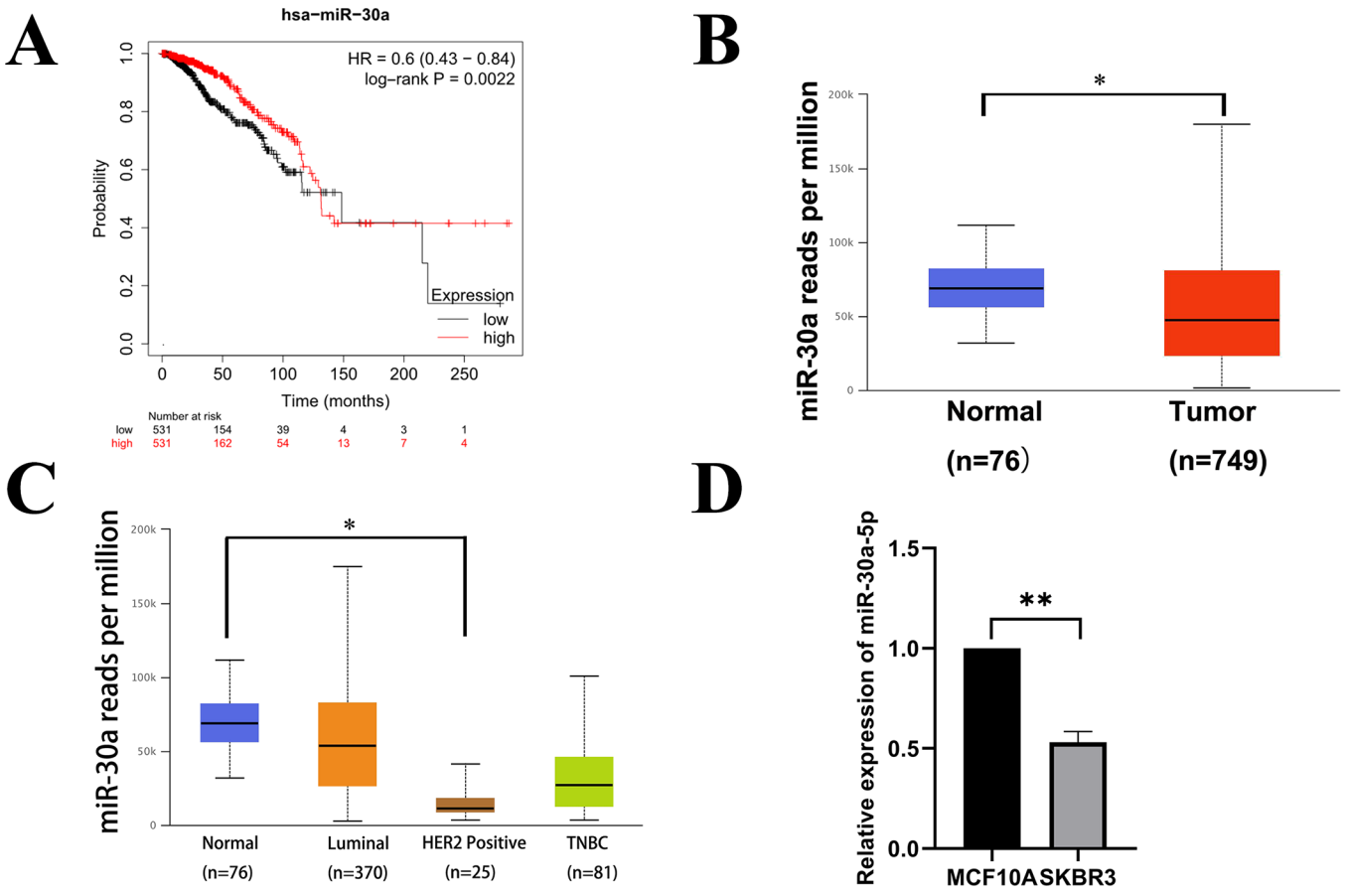

Figure 1. (A) Kaplan−Meier analysis showing overall survival of patients with breast cancer classified according to miR-30a levels. (B) Expression of miR-30a in TCGA database with breast cancer. (C) Expression of miR-30a in TCGA database with different subtypes of breast cancer. (D) Determination of the relative expression levels of miR-30a in normal breast epithelial cells MCF-10A and breast cancer cells SKBR3 by qRT-PCR. Data represent mean ± SD (n = 3), *p < 0.05, **p < 0.01.

resuspend the RNA, while the RNA concentration and purity were measured using NanoDrop One (Thermo, USA) to calculate the RNA mass used for cDNA preparation. For miR-30a-5p, 2 μg of cDNA was prepared by reverse transcription. cDNA was diluted onefold by adding RNase-free H_2O, and qRT-PCR reaction was conducted using U6 snRNA as control. Both reverse transcription and qRT-PCR were performed using All-in-One miRNA qRT-PCR Detection Kit 2.0; for SNAI1, 2 μg of cDNA was prepared by reverse transcription using HiScript III RT SuperMix. cDNA was diluted onefold by adding RNase-free H_2O, and β-actin was used as a control, while qRT-PCR reactions were performed using All-in-One qRT-PCR Mix. The relative mRNA expression was determined by the $2^{\wedge(-\Delta\Delta Ct)}$ method according to the cycling threshold (CT) of each group.

2.12. Western Blot Assay. SKBR3 cells were seeded in six-well plates at a density of 10^5/well for 12 h and then treated with free miR-30a, LDH@NC, or LDH@miR-30a (100 nM/2 mL, based on miR-30a concentration, diluted with complete medium) for 48 h. Cells were collected after digestion with 0.25% trypsin and washed with PBS. Using RIPA with PMSF to prepare protein lysis solution (RIPA: PMSF = 99:1), the cells were lysed at 4 °C for 30 min. Total protein was collected by centrifugation at 12,000 rpm for 15 min at 4 °C, and the concentration was determined using the BCA protein assay kit. Equal amounts of total protein (35 μg) were then analyzed by 10% SDS-PAGE electrophoresis and transferred PVDF membranes. Primary antibodies were incubated overnight (about 12 h) at 4 °C after samples were blocked with 5% skimmed milk. Blots were incubated with HRP-labeled secondary antibodies for 2 h at room temperature. Finally, the PVDF membrane was detected by the chemiluminescent HRP substrate. Images were analyzed using the ChemiDoc XRS$^+$ system (Bio-Rad, USA). Protein bands were analyzed using ImageJ 1.51j8 (64-bit) software. All grayscale values were normalized to that of β-actin or GAPDH for statistical evaluation.

2.13. Mouse Xenotransplantation Assay. The xenograft tumor model was generated by subcutaneous injection of 5 × 10^5 SKBR3 cells/100 μL in PBS into the right flank region of the mice. When the tumor volume reached 100 mm^3 (at day 7), the mice were randomly assigned to four groups of four mice each, and the control (100 μL PBS), LDH, miR-30a, and LDH@miR-30a were injected intratumorally at a dose of 1.5 nmol per mouse per session, respectively. The treatment was repeated every other day for a total of five treatments. Tumor volume was monitored according to the following formula: $V = 1/2LW^2$ (L and W are the length and width of the tumor, respectively). Tumor volume and body weight were measured every 2 days during 10 days.

2.14. Hematoxylin−Eosin (H&E) and TUNEL Staining. On day 10, the mice in each group were sacrificed. For H&E staining, the major organ of mice was collected, fixed in 4% paraformaldehyde overnight, and embedded in paraffin according to standard histological protocols. Next, the tissue

https://doi.org/10.1021/acsomega.2c07866
ACS Omega 2023, 8, 18435−18448

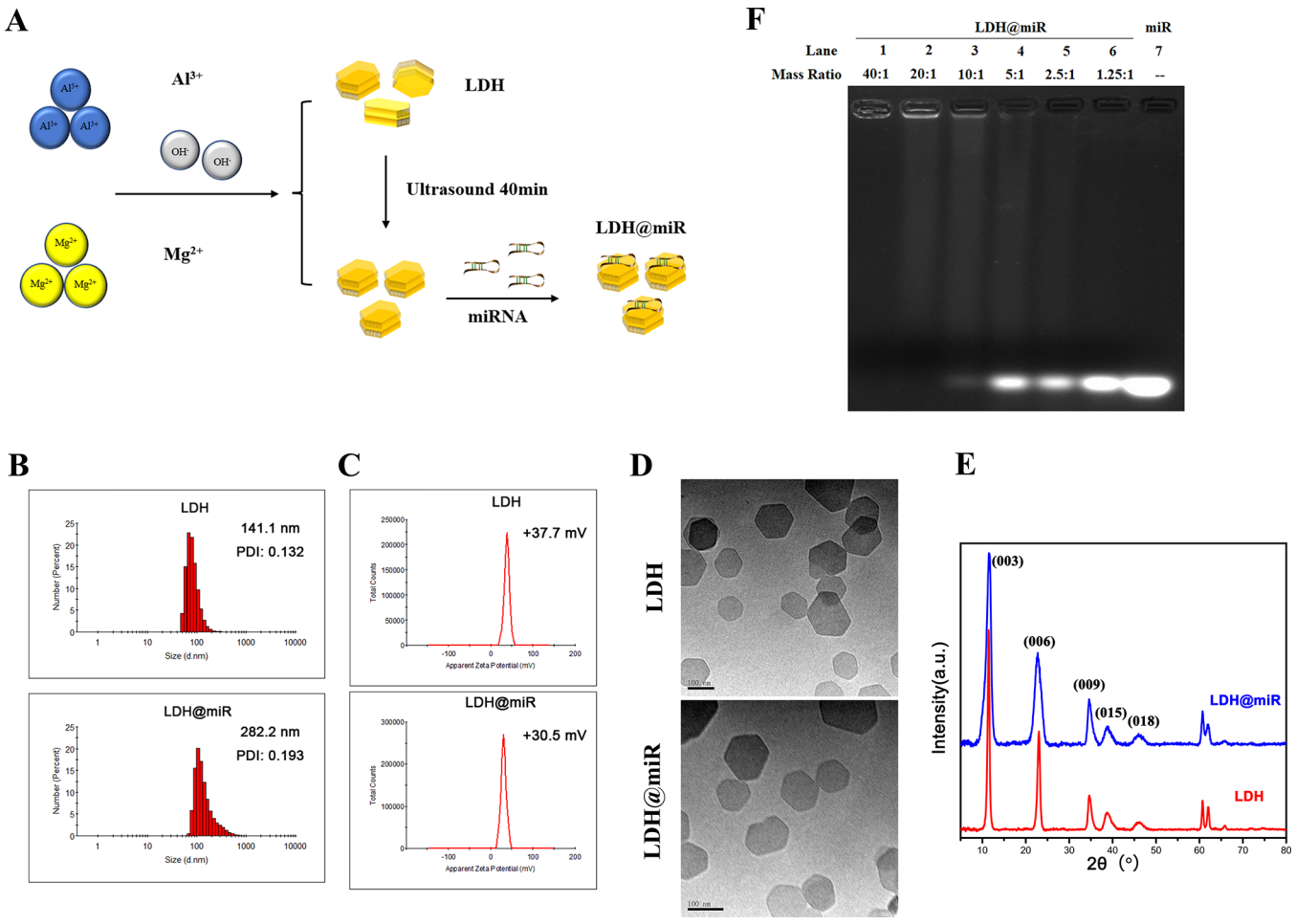

Figure 2. (A) Preparation and characterization of LDH@miR-30a. (B) Particle size distribution of LDH and LDH@miR-30a NPs. (C) Zeta potential of LDH and LDH@miR-30a at 25 °C. (D) TEM images of LDH and LDH@miR-30a. Scale bars: 100 nm. (E) XRD pattern of LDH and LDH@miR-30a. (F) miR-30a loading capacity detected by agarose gel electrophoresis.

was cut into 5 μm-thick cross-sectional slices. The paraffin sections in each group were dewaxed, stained with hematoxylin for 3−5 min, and differentiated with ethanolic hydrochloric acid. The paraffin sections were washed and stained with eosin for 5 min. Images were photographed under a microscope (Eclipse C1, Nikon, Japan).

For TUNEL staining, the harvested tumor tissues were first fixed with 4% paraformaldehyde. Then, they were embedded in an optimal cutting temperature compound followed by cutting into 5 μm-thick sections. The sections were treated using Triton X-100 at room temperature for 10 min and then blocked with 5% bovine serum albumin. The apoptotic cells were measured with a TUNEL apoptosis assay kit in accordance with the manufacturer's instruction. DAPI was selected for nuclear staining. The image was photographed under a microscope (Eclipse C1, Nikon, Japan).

2.15. Statistical Analysis. All data were collected from experiments that were performed at least three times and we expressed as the mean ± standard deviation (SD). The results were analyzed using one-way ANOVA with SPSS 25.0 software, followed by comparisons using t test. The significant difference was labeled as $^{*}p < 0.05$, $^{**}p < 0.01$, and $^{***}p < 0.001$.

3. RESULTS

3.1. MiR-30a Is Downregulated in Breast Cancer and Positively Correlates with Patient Survival. Statistical analysis of the overall survival of 1062 BC patients in TCGA by KM Plotter (Figure 1A) showed that BC patients with low miR-30a expression have a lower survival rate and poor prognosis, $p < 0.01$. Difference analysis showed that miR-30a expression was significantly higher in normal breast tissue than BC (Figure 1B), and miR-30a expression is significantly different between normal breast tissue and HER2-positive BC (Figure 1C). In addition, the qRT-PCR results (Figure 1D) revealed that miR-30a expression was significantly lower in SKBR3 BC cells (HER2-positive) than in MCF-10A normal breast epithelial cells.

3.2. Physicochemical Characterization of LDH@miR-30a NPs. We first synthesized LDH through the coprecipitation method. Then, cationic LDHs were mixed with miR-30a at room temperature for 1 h to obtain LDH@miR-30a (Figure 2A). The surface charge and size of nanoparticles are important parameters affecting the loading of miRNA. As shown in Figure 2B, LDH@miR-30a had a mean hydrodynamic diameter about 282.2 nm with the polydispersity index at 0.193, which indicated good uniformity of nanoparticles. As shown in Figure 2C, LDH@miR-30a showed a zeta potential at +30.3 mV, which not only indicated successful loading of miR but also exhibited a moderate potential to be internalized easily by cell membranes, which presented negative charges. The TEM image showed that LDH@miR-30a had a narrow distribution and dispersed uniform morphology based on regular hexagon (Figure 2D). LDH@miR-30a exhibited the same XRD pattern compared with

https://doi.org/10.1021/acsomega.2c07866
ACS Omega 2023, 8, 18435−18448

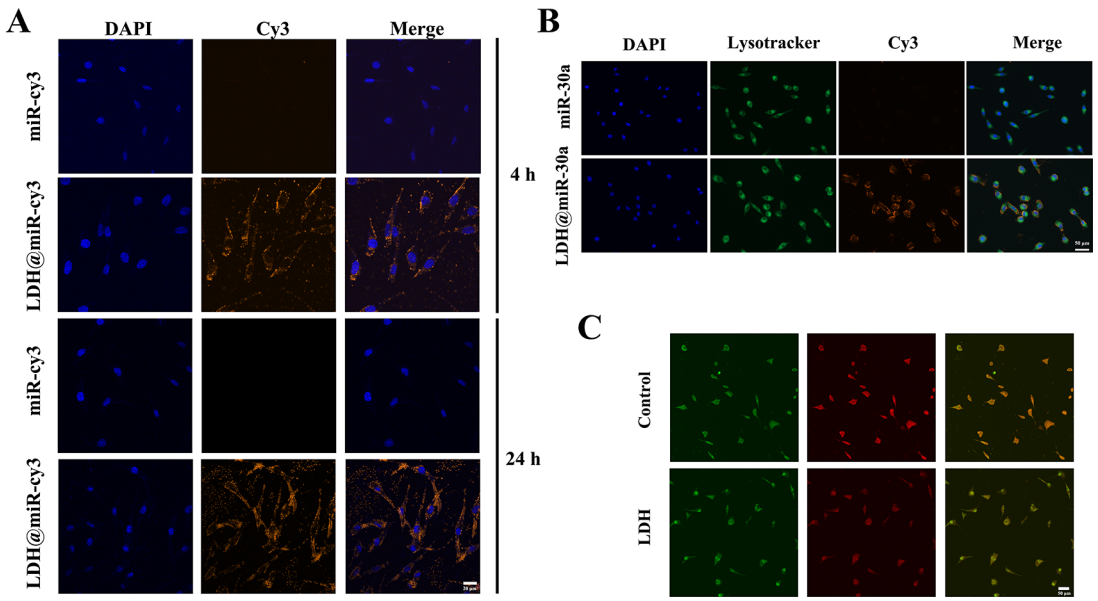

Figure 3. (A) Fluorescence microscopy images of free miR-Cy3 and LDH@miR-Cy3 uptake by SKBR3 cells after 4 h and 24 h of incubation [60× magnification]. Scale bars: 20 μm. (B) Intracellular colocalization of LDH@miR-Cy3 and miR-Cy3 in SKBR3 cells after 4 h of incubation, and labeled with DAPI (blue) and Lysotracker (green) to distinguish cell nuclei and lysosome, respectively [20× magnification]. Scale bars: 50 μm (C) Fluorescence microscopy images of SKBR3 cells treated with LDH, indicating lysosomal membrane damage, [20× magnification] Scale bars: 50 μm.

LDH, as reflected by typical reflections of (003), (006), (009), (015), and (018) planes (Figure 2E).

The miRNA condensation capability of particle is crucial in nanoparticle-based miRNA delivery. Therefore, the saturation of the miR-30a binding to LDH was assessed by agarose gel retardation assay. As shown in Figure 2F, the miRNA condensation ability was measured at different LDH to miR-30a mass ratios, and the result manifested that miR-30a was retarded in spotting holes entirely at the mass ratio of 40, suggesting that miR-30a could be carried completely by LDH. Based on the results of cell function experiments, we chose to use an LDH to miRNA mass ratio of 10:1 in subsequent experiments.

3.3. Cellular Uptake and Intracellular Localization of LDH@miR-30a. To assess the ability of LDH@miR-30a to be taken up by SKBR3 cells, we performed experiments using miR-30a-Cy3 loaded on LDH nanomaterials, and the results showed that naked miRNA did not appear in SKBR3 cells. In contrast, LDH@miR-30a could be successfully taken up by SKBR3 cells, and after 24 h it remained stable in the cytoplasm (Figure 3A). We speculate that LDH@miR-30a can escape from lysosomal breakdown. To explore it, we used Lysotracker Green as a lysosomal dye to label. After 4 h incubation, the SKBR3 cell treated with LDH@miR-30a showed a clear orange fluorescence in the cytoplasm (Figure 3B), indicating that LDH@miR-30a was not catabolized by lysosomes after entering the cells via endocytosis. However, free miRNA was difficult to enter cells and easy to be captured by lysosome, which is according to a previous report. Therefore, LDH@miR could deliver miRNA efficiently to cytoplasm to exert function, which could enhance bioavailability of miRNA obviously.[24] AO is a lysosomal fluorescent dye that accumulates in acidic organelles in a pH-dependent manner.[25] As shown in Figure 3C, SKBR3 cells with PBS treatment as control showed clear red fluorescence from late endosomes/lysosomes in cells, and SKBR3 cells incubated with LDH for 24 h showed negligible red fluorescence from late endosomes/lysosomes, indicating that late endolysosomal membranes were ruptured upon LDH treatment.

3.4. In Vitro Antitumor Effect of LDH@miR-30a. To evaluate the effect of different formulations on SKBR3 cell viability, we performed cytotoxicity assays at 24 and 48 h, respectively. The LDH nanomaterials had no significant promotion or inhibition of SKBR3 cell viability even at the highest concentration, and cell survival remained above 80% across the concentration range tested. As shown in Figure 4A, free miR-30a only slightly inhibited cell viability, possibly owing to the low efficiency of miRNA transfection in the absence of a vector. However, cell viability was significantly inhibited in the group treated with LDH@miR-30a. Moreover, the inhibitory effect of LDH@miR-30a was significantly higher than free miR-30a at the concentration of 100 nM at 24 h.

3.5. Effects of LDH@miR-30a on Cell Cycle Arrest. In this study, the cell cycle changes of SKBR3 cells treated with LDH@NC, free miR-30a, and LDH@miR-30a were examined using flow cytometry to investigate the mechanism of cytotoxic effects of LDH@miR-30a. Compared to the other groups, the G0/G1 population of cells depicted significant aggregation after LDH@miR-30a treatment, with a proportion of 74.56%; meanwhile, the S-phase population was reduced, with a proportion of 21.49%, demonstrating that the cells were blocked in the transition from the G1 to S phase (Figure 4B,C). Therefore, we speculated that LDH@miR-30a may suppress cell viability through cell cycle arrest. This conclusion is consistent with the in vitro cellular CCK8 assay results.

3.6. Suppression of Migration and Invasion by LDH@miR-30a. We evaluated the effect of LDH@miR-30a on SKBR3 migration using a wound-healing assay. The wound healing area of the control group, free miR-30a group, and LDH@NC group were all over half, whereas the wound healing area of the LDH@miR-30a-treated group was significantly smaller than the other groups (Figure 5C,D). On the other hand, we assessed the effect of LDH@miR-30a on SKBR3 invasion by Transwell assay, and the number of invasive cells in the LDH@miR-30a-treated

https://doi.org/10.1021/acsomega.2c07866
ACS Omega 2023, 8, 18435−18448

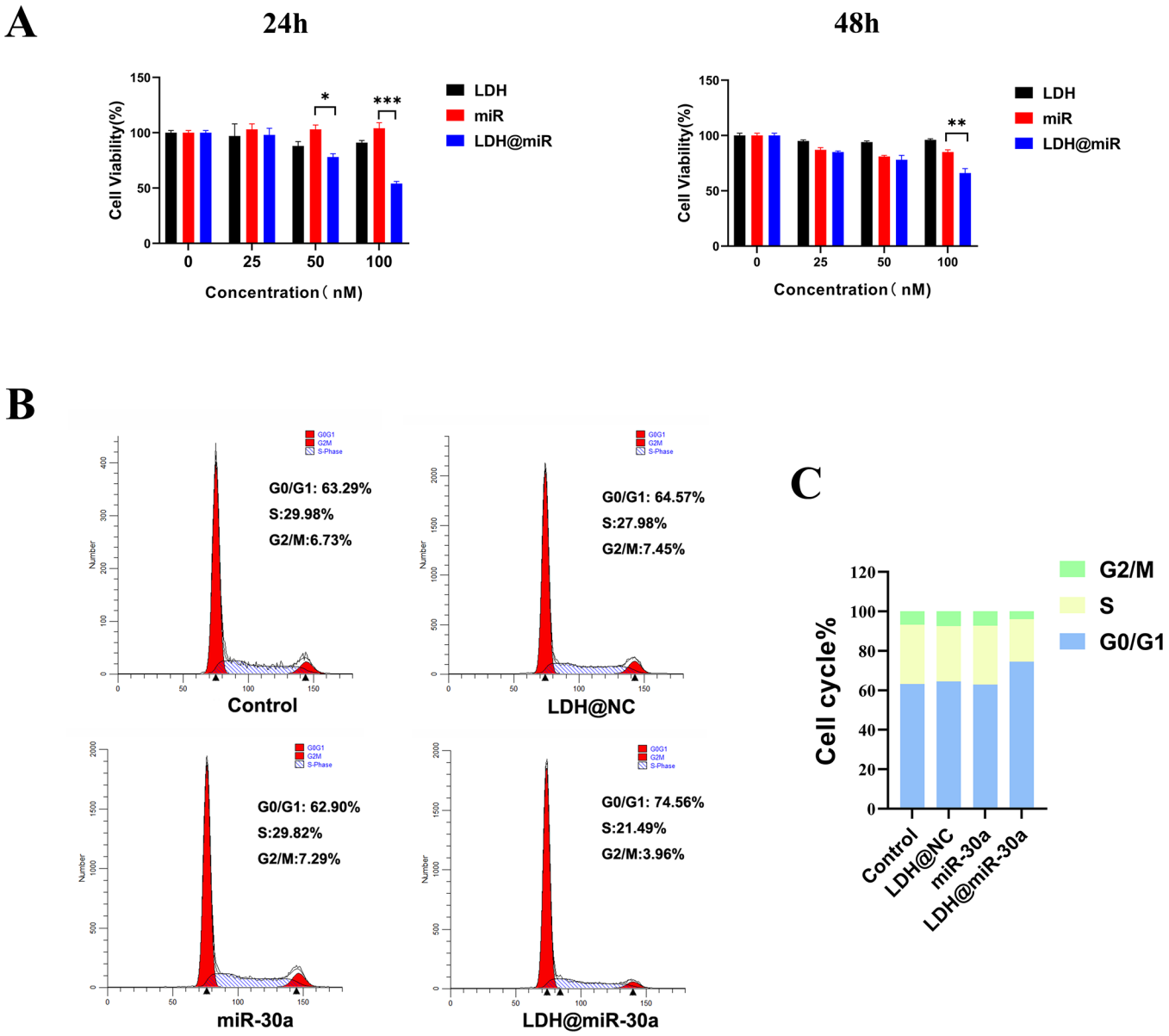

Figure 4. (A) In vitro cell viability assay using CCK8 reagents. The cell viability of SKBR3 cells treated with LDH, free miR-30a, or LDH@miR-30a after 24 and 48 h. (B) Flow cytometry analysis of cell-cycle phase distribution in SKBR3 cells. (C) Histogram showing the cell-cycle distribution after treatment with LDH@NC, miR-30a, and LDH@miR-30a. Data represent mean ± SD (n = 3), *p < 0.05, **p < 0.01, ***p < 0.001.

group was only about half of the other groups (Figure 5A,B). These results suggested that LDH@miR-30a can suppress cell migration and invasion.

3.7. In Vitro Anti-Tumor Mechanism of LDH@miR-30a. In order to evaluate the downstream target genes of miR-30a, which are able to inhibit tumor development in BC, the target gene of miR-30a was screened for using the target gene prediction software TargetScan. The predicted binding site of miR-30a, SNAI1 3′-UTR, is presented in Figure 6A. Among the numerous potential target genes, due to its function in the development of human cancer, SNAI1 was selected as the target gene of interest. SNAI1 is a regulatory factor in the process of EMT in tumor cells. It promotes the occurrence of EMT in tumor cells by upregulating Vimentin and downregulating the expression of E-cadherin.[26] The results of qRT-PCR (Figure 6B) and Western blot (Figure 6C,D) showed that the expression of SNAI1 in SKBR3 cells decreased significantly after LDH@miR-30a treatment. Meanwhile, EMT-associated proteins (E-cadherin, N-cadherin, Vimentin) were detected by Western blot. The results (Figure 7A,B) showed that the expression of EMT-related proteins N-cadherin and Vimentin decreased significantly, and the expression of E-cadherin increased when cells were treated with LDH@miR-30a.

3.8. Antitumor Effect and Biosafety of LDH@miR-30a Nanocarriers In Vivo. To investigate the therapeutic effect of LDH@miR-30a in vivo, we established a xenograft model in nude mice, and the treatment process is shown in Figure 8. The whole treatment process lasted for 10 days, and the tumor volumes were recorded every 2 days. No apparent body weight loss was observed in all groups (Figure 9D), indicating desirable biocompatibility and biosafety of LDH@miR-30a. After a 10-day treatment, all mice were euthanized to obtain photos and tumor weights (Figure 9C,F). The LDH@miR-30a treatment exhibited significant tumor inhibition compared to the PBS group (Figure 9F). The tumor volume in the LDH@miR-30a was only 2.3-fold larger than the initial tumor at 10-day post-

https://doi.org/10.1021/acsomega.2c07866
ACS Omega 2023, 8, 18435−18448

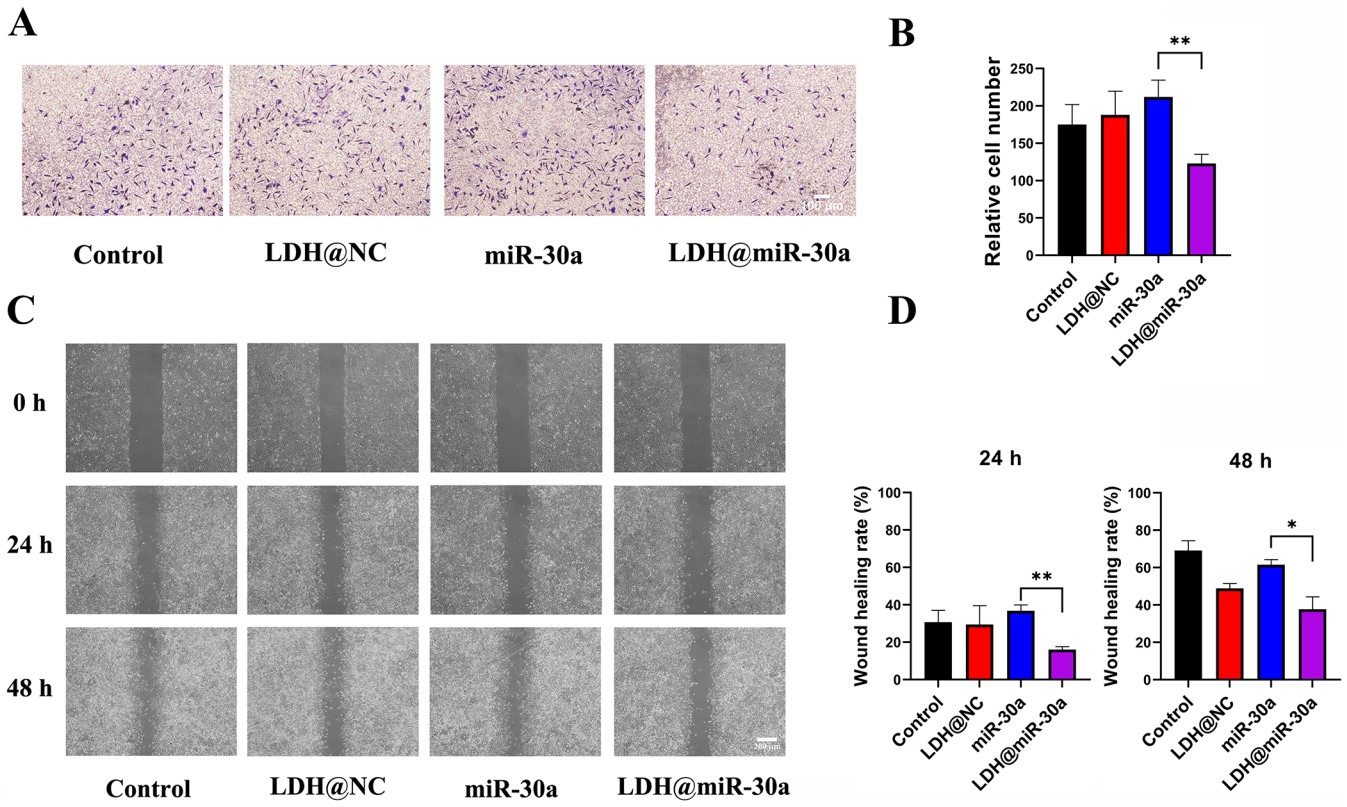

Figure 5. LDH@miR-30a inhibited the migration ability of SKBR3 cells in vitro. (A) Transwell migration assay was used to detect the number of transmembrane cells. Representative microphotographs of the Boyden chamber assay of SKBR3 cells. Scale bars: 100 μm. (B) The bar graphs indicate the number of invasive cells in the different treatment groups. (C) Wound-healing assays were performed to assess cell migration. Cells were treated with LDH@NC, miR-30a, and LDH@miR-30a for 0, 24, and 48 h or untreated. Representative images of treated and untreated cells are shown. Scale bars: 200 μm. (D) Area recovery by cells at 24 and 48 h are shown. Data represent mean ± SD (n = 3), *p < 0.05, **p < 0.01.

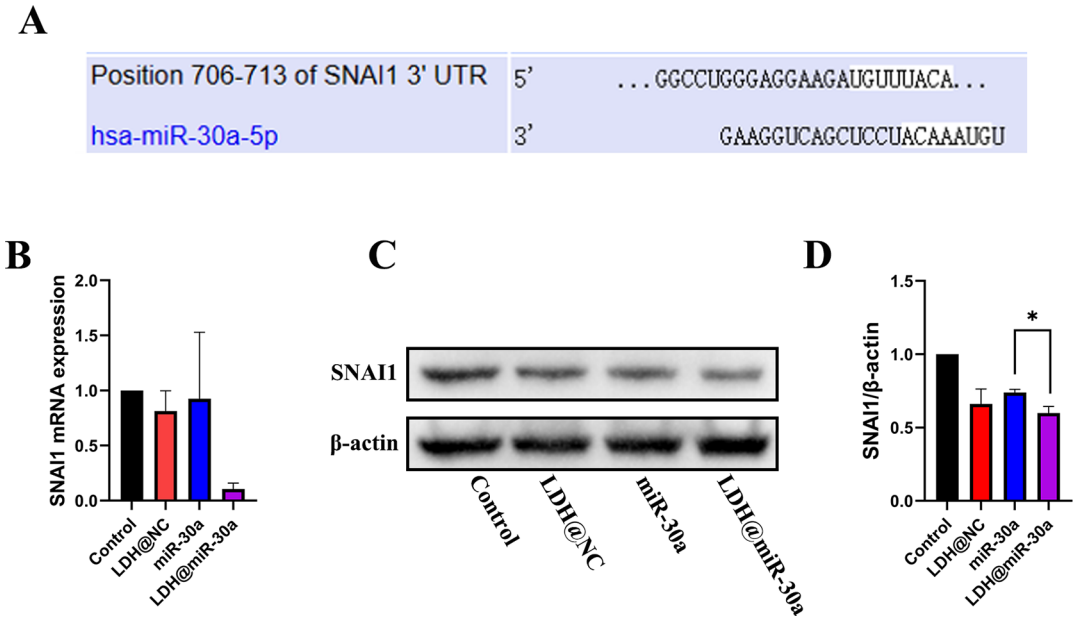

Figure 6. (A) TargetScan predicts that miR-30a-5p may regulate the expression of SNAI1. (B) After SKBR3 cells were treated with LDH, naked miR-30a, or LDH@miR-30a, and the mRNA expression levels of SNAI1 were detected by qRT-PCR. (C, D) After SKBR3 cells were treated with LDH, naked miR-30a, or LDH@miR-30a, the protein expression levels of SNAI1 were detected by Western blot. Data represent mean ± SD (n = 3), *p < 0.05.

treatment, while the free miR-30a group showed an eightfold increase in the tumor volume.

The HE staining and the terminal TUNEL assay of the sections were performed post treatment. Histopathology analysis showed that no obvious signs of abnormality were

https://doi.org/10.1021/acsomega.2c07866
ACS Omega 2023, 8, 18435−18448

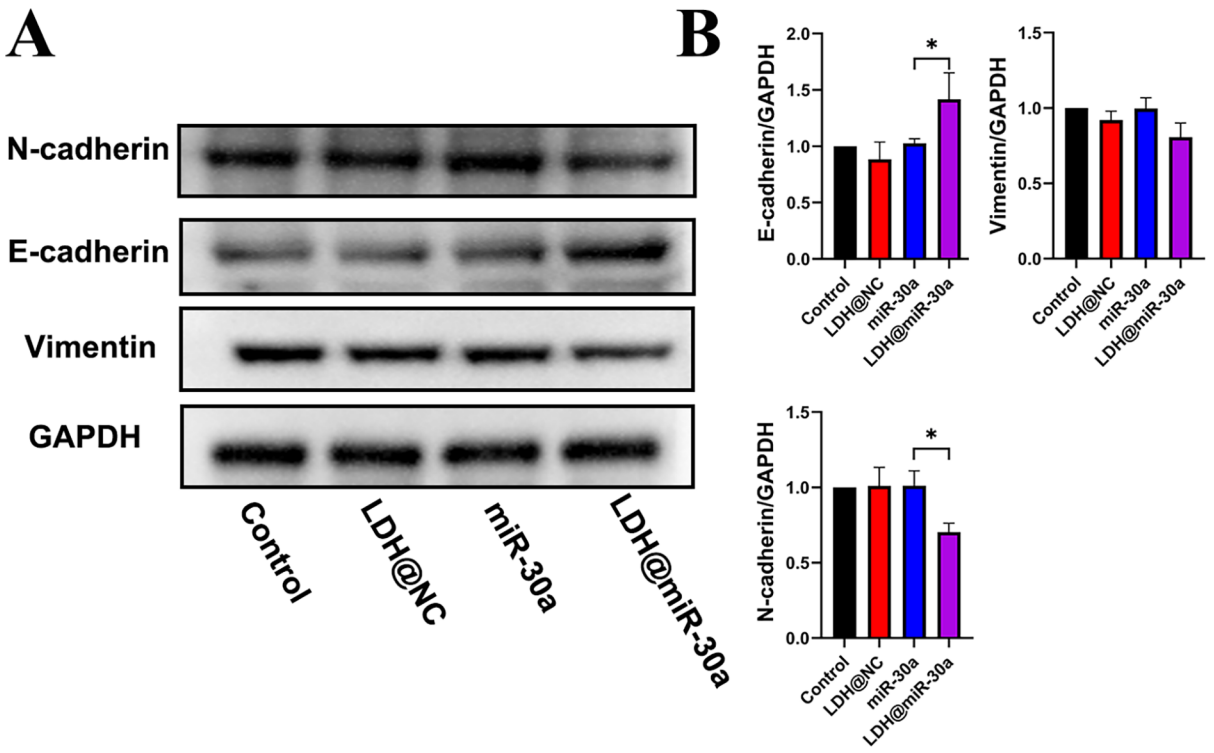

Figure 7. (A, B) Expression levels of E-cadherin, N-cadherin, and Vimentin of SKBR3 cells treated with LDH, naked miR-30a, or LDH@miR-30a were analyzed by Western blot. GAPDH served as a loading control. Data represent mean ± SD (n = 3), *p < 0.05.

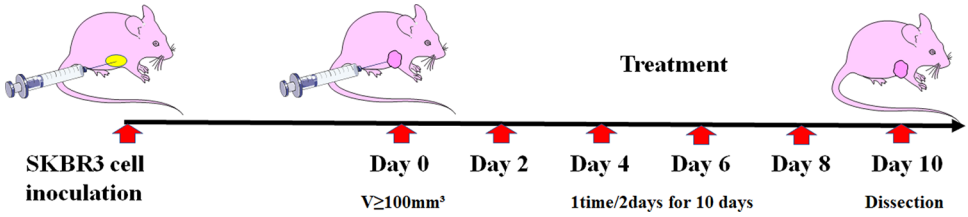

Figure 8. Flowchart of LDH@miR-30a in vivo treatment of xenograft tumor.

observed in the major organs (heart, liver, spleen, and kidney) in each group, further demonstrating that LDH nanoparticles were of excellent biosafety (Figure 10A).

Also, the in situ TUNEL assay visibly exhibited substantial cell apoptosis after treatment via LDH@miR-30a, among which the bright-green fluorescence stands for the apoptotic cells and the LDH@miR-30a group shows the higher rate of apoptotic cells than other groups (Figure 10B).

4. DISCUSSION

As one of the cancer therapeutic approaches, RNAi has abundant candidate targets as well as wide distribution of indications and plays an important role in regulating the gene expression of tumor cells. Numerous studies have shown that miR-30a can negatively regulate the development of BC; for example, miR-30a can target Smad2,[27] ZEB2,[28] and MTDH[11] to suppress BC metastasis and invasion. The miR-30a/Eya2 axis could regulate G1/S cell-cycle progression and suppresses BC cell proliferation and migration by targeting Eya2.[13] miR-30a has also been shown to enhance the sensitivity of BC to chemotherapeutic agents and improve tumor resistance by reducing Beclin 1-mediated autophagy.[29,30] Kawaguchi et al. reported that high miR-30a expression levels were significantly associated with overall survival in ER-positive (p = 0.0001) and non-triple-negative (p = 0.0168) BC patients.[12] Xiao have reported that miR-30a was able to affect the proliferation and invasion of BC cells by regulating SNAI1 expression.[31] Therefore, we queried TCGA database and found that miR-30a was down-regulated in BC and validated this finding in qRT-PCR experiment. In addition, we found that BC patients with low miR-30a expression had a lower overall survival rate and a poorer prognosis.

However, the instability of RNA itself is one of the main obstacles to its application in cancer treatment, as it is easily decomposed by RNA enzymes in vivo and easily eliminated by the kidney.[32] MiRNA-conjugated nanoparticles have superior delivery efficiency compared to free miRNA.[33] For example, Shu et al. used nanoparticles constructed from pRNA-3WJ core to bind to epidermal growth factor receptor (EGFR) aptamers to deliver anti-miR-21 for the treatment of triple-negative BC in vitro and in vivo;[34] Yang et al. developed the polyethyleneimine-modified dendritic mesoporous silica nanoparticles loaded with microRNA-125a (DMSN-PEI@125a) that reversed the immunosuppression of the tumor microenvironment and inhibited TC-1 tumor growth.[35] Nguyen et al. prepared nanoparticles that deliver miRNA to mouse macrophages based on biodegradable chitosan derivatives, which can regulate ABCA1 expression and cholesterol efflux, hence modulating atherosclerotic lesions.[36] In

https://doi.org/10.1021/acsomega.2c07866
ACS Omega 2023, 8, 18435−18448

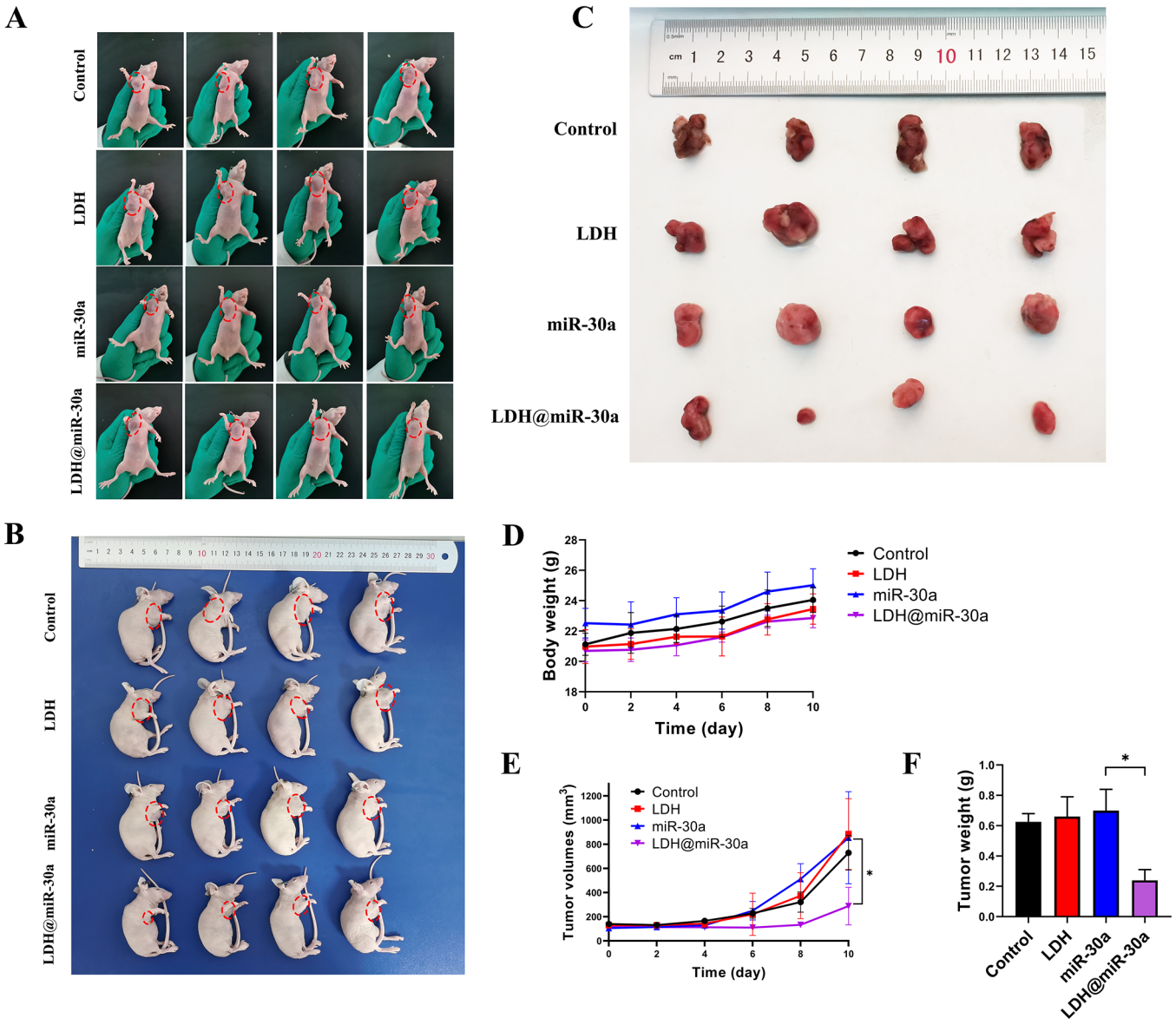

Figure 9. (A) Pictures of subcutaneous implant tumors in naked mice on day 10 of different treatment groups. (B) The tumor growth status of each treatment group after 10 days of treatment. (C) The tumor volumes of different treatment groups were photographed after 10 days of treatment. (D) Curves of body weight changes over time for different treatment groups of nude mice. (E) Curves of tumor volume growth over time in different treatment groups. (F) Tumor weights of different treatment groups. Data are represented as the mean ± standard deviation (mean ± SD) of four mice per group. *$p < 0.05$.

addition, Gajda et al. loaded miR-7-5p and drugs in combination into monoolein cubosomes and treated human glioma cells, papillary thyroid cells, and cervical cancer cells in vitro, effectively increasing drug sensitivity and decreasing expression of multidrug resistance (MDR)-associated genes among these cells.[37]

This study used LDH nanomaterials as a gene-drug delivery system to load miR-30a. As a non-viral gene delivery vehicle, the positive surface charge of LDH facilitates effective penetration of cell membranes,[38] and the excellent anion exchange capacity of LDH allows for easy insertion of negatively charged functional biomolecules into its interlayer region, enabling it to carry and deliver anionic biomolecules and drugs.[39,40] Ladewig et al. successfully used LDH to deliver siRNA into mammalian cells to achieve transient knockdown of target genes;[20] Yoo et al. used LGdH, a number of the LDH, as a vector to load miR-10b inhibitor, which enhanced HOXD10 expression and inhibited MDA-MB-231 cell invasion in vitro;[41] Yang et al. used LDH to carry let-7d to synergistically regulate BMSCs toward osteoblastic direction and demonstrated enhanced osteogenic ability in a subcutaneous ectopic osteogenesis model in nude mice.[42] Yang et al. regulated the tumor microenvironment (ITM) by repolarizing tumor-associated macrophages (TAMs) to the M1 subtype via LDH@miR155 and confirmed this in vivo in tumor-bearing C57BL/6 J mice.[22]

This study used a 1:10 mass ratio of miRNA:LDH nanoparticles sufficient to cover the majority of nucleic acids to LDH, thus allowing the negative charge of miRNA to be effectively masked and remain in the gel wells rather than migrating toward the positive electrode in the gel electrophoresis device as is the case with naked miRNA.

https://doi.org/10.1021/acsomega.2c07866
ACS Omega 2023, 8, 18435−18448

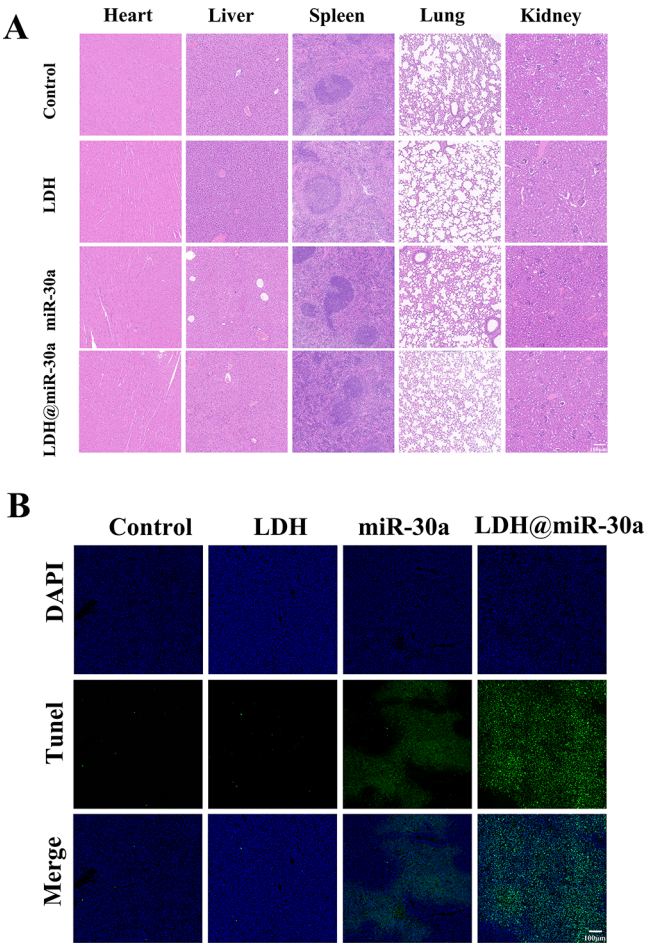

Figure 10. (A) Representative H&E staining images of vital organs sections, including heart, liver, spleen, lungs, and kidneys, scale bars: 100 μm. (B) Representative TUNEL staining images of tumor sections of different groups of mice, scale bars: 100 μm.

Because of the small size and positive charge of LDH@miR-30a, it can be effectively taken up by SKBR3 cells. The orange fluorescence of miR-Cy3 can be detected in the cytoplasm after 4 h, and the fluorescence intensity in the cytoplasm is still high after 24 h. Meanwhile, we found that LDH@miR-30a could escape the lysosomal pathway and the results of AO staining experiments demonstrated that the LDH material itself could increase the permeability of lysosomes. We hypothesized that the mechanism of LDH@miR-30a uptake by SKBR3 cells is that LDH@miR-30a enters the cell by cytokinesis and the LDH vectors trigger the proton sponge effect through its decomposition to buffer the endosomal acidic environment,[43,44] thus avoiding the lysosomal pathway delivering the loaded miR-30a into the cytoplasm of the cell, which enhances the transfection efficiency of miRNAs. This demonstrates the higher biological availability of LDH@miR-30a compared to naked miRNAs.

LDH, as a gene delivery system, has no significant promotion or inhibition of the proliferation of BC SKBR3 cells by itself. In contrast, LDH@miR-30a could significantly inhibit SKBR3 cell proliferation, and the inhibitory effect was significantly higher than free miR-30a. We performed cell cycle assays using flow cytometry for different treatment groups and demonstrated that LDH@miR-30a induced SKBR3 cells to arrest at the G0/G1 phase.

During the development of tumor cells, the loss of some epithelial cell properties and the acquisition of some mesenchymal cell properties through EMT also allows the gain of more important invasive and detachment capabilities.[45] During EMT progression, epithelial cell polarity is lost, contact with surrounding cells and stromal cells is reduced, intercellular interactions are reduced, cell migration and mobility are enhanced, cell phenotype is altered, and epithelial phenotype is lost. SNAI1, as a regulator of tumor EMT progression, is highly correlated with tumor cell invasion, metastasis, and recurrence by abnormal expression.[46] Previous papers have reported that the 3′-UTR of SNAI1 mRNA is a direct target of miR-30a in BC cells, and miR-30a can inhibit SNAI1 expression, thus suppressing the invasiveness of BC.[31,47,48]

As a suppressor oncogene, E-cadherin mediates cell adhesion and maintains integrity.[49] During cancer progression, reduced E-cadherin levels can lead to reduced cell adhesion, and its frequent downregulation is associated with aggressive tumor behavior and poor prognosis.[50,51] In contrast, overexpression of SNAI1 can reduce E-cadherin expression.[52,53] SNAI1 has been found to reduce E-cadherin expression by interacting with the E-box near the E-cadherin promoter and enhancing Vimentin expression to induce EMT progression.[51,54] Vimentin is required to maintain the cytoplasmic structure, and abnormal Vimentin expression during EMT contributes to epithelial plasticity and tumor cell metastasis.[15] N-cadherin is found in most invasive and metastatic human BC cell lines and tumor overexpressed.[49] In this study, the impacts of LDH@miR-30a on the expression level of SNAI1 in SKBR3 cells was verified by Western blot and qRT-PCR, and the expression of EMT-related proteins was examined. The results demonstrated that LDH@miR-30a could increase the expression of epithelial marker E-cadherin by down-regulating SNAI1, while decreasing the expression of mesenchymal markers (Vimentin, N-cadherin), and cause the cells to regain epithelial properties and achieve the effect of inhibiting BC cell migration and invasion.

We treated nude mice with LDH@miR-30a in a subcutaneous transplantation tumor model and obtained good anti-tumor effects, with noticeably slower tumor progression in the LDH@miR-30 group compared to other experimental groups. Compared with those injected with PBS, the mice injected with LDH@miR-30 presented remarkably more apoptotic cell in tumor tissue. The possible reason for it is that in vivo, the small size of LDH@miR-30a accumulates and stays at the tumor site with the help of tumor vascular leakage and lack of lymphatic drainage (EPR effect) for RNAi treatment.[55] Meanwhile, during the treatment, neither LDH nor LDH@miR-30a caused damage to the heart, liver, spleen, lung, and kidney of mice, demonstrating the good biocompatibility of LDH@miR-30a, which is consistent with the results of in vitro experiments.

However, this study used SKBR3 cells, which were HER2-positive cells and no other BC cell lines were used. We will further explore LDH@miRNA for the treatment of various types of BC in our future work.

5. CONCLUSIONS

In this study, we successfully prepared LDH@miR-30a by using LDH nanomaterials carrying miR-30a and applied LDH@miR-30a to the treatment of BC in vitro and in vivo. We demonstrated that LDH@miR-30a can avoid the lysosomal pathway and deliver miR-30a to BC cells and exert anti-cancer effects. This indicated that LDH@miR-30a is an effective drug delivery system for BC treatment.

https://doi.org/10.1021/acsomega.2c07866
ACS Omega 2023, 8, 18435−18448

AUTHOR INFORMATION

Corresponding Authors

Changjie Chen − *Department of Biochemistry, School of Laboratory Medicine, Bengbu Medical College, Bengbu, Anhui 233030, China*; Email: tochenchangjie@163.com

Qingling Yang − *Department of Biochemistry, School of Laboratory Medicine, Bengbu Medical College, Bengbu, Anhui 233030, China*; Email: yqlmimi@163.com

Wenrui Wang − *Anhui Province Key Laboratory of Translational Cancer Research, Department of Life Science, Bengbu Medical College, Bengbu, Anhui 233030, China*; Email: wenrui-wang1983@163.com

Authors

Shiwen Zhang − *Anhui Province Key Laboratory of Translational Cancer Research, Department of Life Science, Bengbu Medical College, Bengbu, Anhui 233030, China*; orcid.org/0000-0002-8146-2420

Siyan Pang − *Anhui Province Key Laboratory of Translational Cancer Research, Department of Life Science, Bengbu Medical College, Bengbu, Anhui 233030, China*

Wenhao Pei − *Anhui Province Key Laboratory of Translational Cancer Research, Department of Life Science, Bengbu Medical College, Bengbu, Anhui 233030, China*

Haitao Zhu − *Department of Biochemistry, School of Laboratory Medicine, Bengbu Medical College, Bengbu, Anhui 233030, China*

Yingxiang Shi − *Department of Biochemistry, School of Laboratory Medicine, Bengbu Medical College, Bengbu, Anhui 233030, China*

Ziyang Liu − *Anhui Province Key Laboratory of Translational Cancer Research, Department of Life Science, Bengbu Medical College, Bengbu, Anhui 233030, China*

Lingyu Mao − *Anhui Province Key Laboratory of Translational Cancer Research, Department of Life Science, Bengbu Medical College, Bengbu, Anhui 233030, China*

Xiuru Shi − *Department of Biochemistry, School of Laboratory Medicine, Bengbu Medical College, Bengbu, Anhui 233030, China*

Shuang Tao − *Department of Biochemistry, School of Laboratory Medicine, Bengbu Medical College, Bengbu, Anhui 233030, China*

Chenchen Geng − *Anhui Province Key Laboratory of Translational Cancer Research, Department of Life Science, Bengbu Medical College, Bengbu, Anhui 233030, China*

Sulian Chen − *Department of Biochemistry, School of Laboratory Medicine, Bengbu Medical College, Bengbu, Anhui 233030, China*

Linnan Yang − *The Centre for Scientific Research of the First Affiliated Hospital of Anhui Medical University, Hefei, Anhui 230022, China*

Complete contact information is available at: https://pubs.acs.org/10.1021/acsomega.2c07866

Author Contributions

#S.Z., S.P., and W.P. have contributed equally to this work.

Author Contributions

W.W., L.Y., and S.Z. conceived the idea of the study. S.Z. drafted the manuscript. S.Z., S.P., W.P., H.Z., Y.S., L.M., and X.S. have performed the most experiments and analyzed the data. S.Z., S.P., Z.L., and S.C. performed the data analyses. W.W. and S.Z. did the final approval of the revised version. W.W., Q.Y., C.C., and L.Y. provided financial support for this study.

Funding

This work was supported by the 512 Talent Cultivation Program of Bengbu Medical College (by51201206), the Nature Science Research Project of Anhui Province (2108085MH294), Anhui Natural Science Foundation (2108085QC107), the University Synergy Innovation Program of Anhui Province (GXXT-2022-064), Anhui Province Key Laboratory of Translational Cancer Research, Medical College (KFZZ202202), the Natural Science Foundation of Bengbu Medical College (2020bypd005), and the Postgraduate Research Innovation Program of Bengbu Medical College (Byycxz21053).

Notes

The authors declare no competing financial interest.

The animal study was reviewed and approved by the Experimental Animal Management and Ethics Committee and Ethics Committee of Bengbu Medical College, Anhui Province, China, Ethics Number: [2022] No. 147.

REFERENCES

(1) Siegel, R. L.; Miller, K. D.; Fuchs, H. E.; Jemal, A. Cancer Statistics, 2022. *Ca-Cancer J. Clin.* **2022**, *72*, 7−33.

(2) Ferlay, J.; Colombet, M.; Soerjomataram, I.; Mathers, C.; Parkin, D. M.; Piñeros, M.; Znaor, A.; Bray, F. Estimating the Global Cancer Incidence and Mortality in 2018: GLOBOCAN Sources and Methods. *Int. J. Cancer* **2019**, *144*, 1941−1953.

(3) Goldhirsch, A.; Winer, E. P.; Coates, A. S.; Gelber, R. D.; Piccart-Gebhart, M.; Thürlimann, B.; Senn, H.-J.; Albain, K. S.; André, F.; Bergh, J.; Bonnefoi, H.; Bretel-Morales, D.; Burstein, H.; Cardoso, F.; Castiglione-Gertsch, M.; Coates, A. S.; Colleoni, M.; Costa, A.; Curigliano, G.; Davidson, N. E.; di Leo, A.; Ejlertsen, B.; Forbes, J. F.; Gelber, R. D.; Gnant, M.; Goldhirsch, A.; Goodwin, P.; Goss, P. E.; Harris, J. R.; Hayes, D. F.; Hudis, C. A.; Ingle, J. N.; Jassem, J.; Jiang, Z.; Karlsson, P.; Loibl, S.; Morrow, M.; Namer, M.; Kent Osborne, C.; Partridge, A. H.; Penault-Llorca, F.; Perou, C. M.; Piccart-Gebhart, M. J.; Pritchard, K. I.; Rutgers, E. J. T.; Sedlmayer, F.; Semiglazov, V.; Shao, Z. M.; Smith, I.; Thürlimann, B.; Toi, M.; Tutt, A.; Untch, M.; Viale, G.; Watanabe, T.; Wilcken, N.; Winer, E. P.; Wood, W. C. Personalizing the Treatment of Women with Early Breast Cancer: Highlights of the St Gallen International Expert Consensus on the Primary Therapy of Early Breast Cancer 2013. *Ann. Oncol.* **2013**, *24*, 2206−2223.

(4) Johnson, K. S.; Conant, E. F.; Soo, M. S. Molecular Subtypes of Breast Cancer: A Review for Breast Radiologists. *J. Breast Imaging* **2021**, *3*, 12−24.

(5) Tang, P.; Tse, G. M. Immunohistochemical Surrogates for Molecular Classification of Breast Carcinoma: A 2015 Update. *Arch. Pathol. Lab. Med.* **2016**, *140*, 806−814.

(6) Braicu, C.; Chiorean, R.; Irimie, A.; Chira, S.; Tomuleasa, C.; Neagoe, E.; Paradiso, A.; Achimas-Cadariu, P.; Lazar, V.; Berindan-Neagoe, I. Novel Insight into Triple-Negative Breast Cancers, the Emerging Role of Angiogenesis, and Antiangiogenic Therapy. *Expert Rev. Mol. Med.* **2016**, *18*, No. e18.

(7) Braicu, C.; Raduly, L.; Morar-Bolba, G.; Cojocneanu, R.; Jurj, A.; Pop, L.-A.; Pileczki, V.; Ciocan, C.; Moldovan, A.; Irimie, A.; Eniu, A.; Achimas-Cadariu, P.; Paradiso, A.; Berindan-Neagoe, I. Aberrant MiRNAs Expressed in HER-2 Negative Breast Cancers Patient. *J. Exp. Clin. Cancer Res.* **2018**, *37*, 257.

(8) Liu, L.; Yi, H.; He, H.; Pan, H.; Cai, L.; Ma, Y. Tumor Associated Macrophage-Targeted MicroRNA Delivery with Dual-Responsive Polypeptide Nanovectors for Anti-Cancer Therapy. *Biomaterials* **2017**, *134*, 166−179.

(9) Zhang, B.; Pan, X.; Cobb, G. P.; Anderson, T. A. MicroRNAs as Oncogenes and Tumor Suppressors. *Dev. Biol.* **2007**, *302*, 1−12.

(10) Jiang, L.; Zhang, H.; Tang, J. MiR-30a: A Novel Biomarker and Potential Therapeutic Target for Cancer. *J. Oncol.* **2018**, *2018*, 1−9.

(11) Zhang, N.; Wang, X.; Huo, Q.; Sun, M.; Cai, C.; Liu, Z.; Hu, G.; Yang, Q. MicroRNA-30a Suppresses Breast Tumor Growth and Metastasis by Targeting Metadherin. *Oncogene* **2014**, *33*, 3119−3128.
(12) Kawaguchi, T.; Yan, L.; Qi, Q.; Peng, X.; Gabriel, E. M.; Young, J.; Liu, S.; Takabe, K. Overexpression of Suppressive MicroRNAs, MiR-30a and MiR-200c Are Associated with Improved Survival of Breast Cancer Patients. *Sci. Rep.* **2017**, *7*, 15945.
(13) Fu, J.; Xu, X.; Kang, L.; Zhou, L.; Wang, S.; Lu, J.; Cheng, L.; Fan, Z.; Yuan, B.; Tian, P.; Zheng, X.; Yu, C.; Ye, Q.; Lv, Z. MiR-30a Suppresses Breast Cancer Cell Proliferation and Migration by Targeting Eya2. *Biochem. Biophys. Res. Commun.* **2014**, *445*, 314−319.
(14) Xiong, J.; Wei, B.; Ye, Q.; Liu, W. MiR-30a-5p/UBE3C Axis Regulates Breast Cancer Cell Proliferation and Migration. *Biochem. Biophys. Res. Commun.* **2019**, *516*, 1013−1018.
(15) Cheng, C.-W.; Wang, H.-W.; Chang, C.-W.; Chu, H.-W.; Chen, C.-Y.; Yu, J.-C.; Chao, J.-I.; Liu, H.-F.; Ding, S.; Shen, C.-Y. MicroRNA-30a Inhibits Cell Migration and Invasion by Downregulating Vimentin Expression and Is a Potential Prognostic Marker in Breast Cancer. *Breast Cancer Res. Treat.* **2012**, *134*, 1081−1093.
(16) Wang, X.; Qiu, H.; Tang, R.; Song, H.; Pan, H.; Feng, Z.; Chen, L. MiR-30a Inhibits Epithelial-mesenchymal Transition and Metastasis in Triple-negative Breast Cancer by Targeting ROR1. *Oncol. Rep.* **2018**, 2635.
(17) Xu, C.; Wang, J. Delivery Systems for SiRNA Drug Development in Cancer Therapy. *Asian J. Pharm. Sci.* **2015**, *10*, 1−12.
(18) Chitkara, D.; Singh, S.; Mittal, A. Nanocarrier-Based Co-Delivery of Small Molecules and SiRNA/MiRNA for Treatment of Cancer. *Ther. Delivery* **2016**, *7*, 245−255.
(19) Lu, M.; Shan, Z.; Andrea, K.; MacDonald, B.; Beale, S.; Curry, D. E.; Wang, L.; Wang, S.; Oakes, K. D.; Bennett, C.; Wu, W.; Zhang, X. Chemisorption Mechanism of DNA on Mg/Fe Layered Double Hydroxide Nanoparticles: Insights into Engineering Effective SiRNA Delivery Systems. *Langmuir* **2016**, *32*, 2659−2667.
(20) Ladewig, K.; Niebert, M.; Xu, Z. P.; Gray, P. P.; Lu, G. Q. M. Efficient SiRNA Delivery to Mammalian Cells Using Layered Double Hydroxide Nanoparticles. *Biomaterials* **2010**, *31*, 1821−1829.
(21) Acharya, R.; Chakraborty, M.; Chakraborty, J. Prospective Treatment of Parkinson's Disease by a SiRNA−LDH Nanoconjugate. *MedChemComm* **2019**, *10*, 227−233.
(22) Yang, L.; Sun, J.; Liu, Q.; Zhu, R.; Yang, Q.; Hua, J.; Zheng, L.; Li, K.; Wang, S.; Li, A. Synergetic Functional Nanocomposites Enhance Immunotherapy in Solid Tumors by Remodeling the Immunoenvironment. *Adv. Sci.* **2019**, *6*, 1802012.
(23) Li, L.; Gu, W.; Chen, J.; Chen, W.; Xu, Z. P. Co-Delivery of SiRNAs and Anti-Cancer Drugs Using Layered Double Hydroxide Nanoparticles. *Biomaterials* **2014**, *35*, 3331−3339.
(24) Ladewig, K.; Niebert, M.; Xu, Z. P.; Gray, P. P.; Lu, G. Q. Controlled Preparation of Layered Double Hydroxide Nanoparticles and Their Application as Gene Delivery Vehicles. *Appl. Clay Sci.* **2010**, *48*, 280−289.
(25) Lin, Y.-C.; Lin, J.-F.; Tsai, T.-F.; Chen, H.-E.; Chou, K.-Y.; Yang, S.-C.; Tang, Y.-M.; Hwang, T. I.-S. Acridine Orange Exhibits Photodamage in Human Bladder Cancer Cells under Blue Light Exposure. *Sci. Rep.* **2017**, *7*, 14103.
(26) Sundararajan, V.; Tan, M.; Zea Tan, T.; Pang, Q. Y.; Ye, J.; Chung, V. Y.; Huang, R. Y.-J. SNAI1-Driven Sequential EMT Changes Attributed by Selective Chromatin Enrichment of RAD21 and GRHL2. *Cancers* **2020**, *12*, 1140.
(27) Li, H.; Song, H.; Yuan, X.; Li, J.; Tang, H. MiR-30a Reverses TGF-B2-Induced Migration and EMT in Posterior Capsular Opacification by Targeting Smad2. *Mol. Biol. Rep.* **2019**, *46*, 3899−3907.
(28) Di Gennaro, A.; Damiano, V.; Brisotto, G.; Armellin, M.; Perin, T.; Zucchetto, A.; Guardascione, M.; Spaink, H. P.; Doglioni, C.; Snaar-Jagalska, B. E.; Santarosa, M.; Maestro, R. A P53/MiR-30a/ZEB2 Axis Controls Triple Negative Breast Cancer Aggressiveness. *Cell Death Differ.* **2018**, *25*, 2165−2180.
(29) Zou, Z.; Wu, L.; Ding, H.; Wang, Y.; Zhang, Y.; Chen, X.; Chen, X.; Zhang, C.-Y.; Zhang, Q.; Zen, K. MicroRNA-30a Sensitizes Tumor Cells to Cis-Platinum via Suppressing Beclin 1-Mediated Autophagy. *J. Biol. Chem.* **2012**, *287*, 4148−4156.
(30) Zhu, H.; Wu, H.; Liu, X.; Li, B.; Chen, Y.; Ren, X.; Liu, C.-G.; Yang, J.-M. Regulation of Autophagy by a Beclin 1-Targeted MicroRNA, MiR-30a. *Cancer Cells. Autophagy* **2009**, *5*, 816−823.
(31) Xiao, B.; Shi, X.; Bai, J. MiR-30a Regulates the Proliferation and Invasion of Breast Cancer Cells by Targeting Snail. *Oncol. Lett.* **2019**, *17*, 406−413.
(32) Gandhi, N. S.; Tekade, R. K.; Chougule, M. B. Nanocarrier Mediated Delivery of SiRNA/MiRNA in Combination with Chemotherapeutic Agents for Cancer Therapy: Current Progress and Advances. *J. Controlled Release* **2014**, *194*, 238−256.
(33) Awasthi, R.; Rathbone, M. J.; Hansbro, P. M.; Bebawy, M.; Dua, K. Therapeutic Prospects of MicroRNAs in Cancer Treatment through Nanotechnology. *Drug Delivery Transl. Res.* **2018**, *8*, 97−110.
(34) Shu, D.; Li, H.; Shu, Y.; Xiong, G.; Carson, W. E.; Haque, F.; Xu, R.; Guo, P. Systemic Delivery of Anti-MiRNA for Suppression of Triple Negative Breast Cancer Utilizing RNA Nanotechnology. *ACS Nano* **2015**, *9*, 9731−9740.
(35) Yang, L.; Li, F.; Cao, Y.; Liu, Q.; Jing, G.; Niu, J.; Sun, F.; Qian, Y.; Wang, S.; Li, A. Multifunctional Silica Nanocomposites Prime Tumoricidal Immunity for Efficient Cancer Immunotherapy. *J. Nanobiotechnol.* **2021**, *19*, 328.
(36) Nguyen, M.-A.; Wyatt, H.; Susser, L.; Geoffrion, M.; Rasheed, A.; Duchez, A.-C.; Cottee, M. L.; Afolayan, E.; Farah, E.; Kahiel, Z.; Côté, M.; Gadde, S.; Rayner, K. J. Delivery of MicroRNAs by Chitosan Nanoparticles to Functionally Alter Macrophage Cholesterol Efflux in Vitro and in Vivo. *ACS Nano* **2019**, *13*, 6491−6505.
(37) Gajda, E.; Godlewska, M.; Mariak, Z.; Nazaruk, E.; Gawel, D. Combinatory Treatment with MiR-7-5p and Drug-Loaded Cubosomes Effectively Impairs Cancer Cells. *Int. J. Mol. Sci.* **2020**, *21*, 5039.
(38) Ladewig, K.; Xu, Z. P.; Lu, G. Q. Layered Double Hydroxide Nanoparticles in Gene and Drug Delivery. *Expert Opin. Drug Delivery* **2009**, *6*, 907−922.
(39) Wu, Y.; Gu, W.; Chen, C.; Do, S. T.; Xu, Z. P. Optimization of Formulations Consisting of Layered Double Hydroxide Nanoparticles and Small Interfering RNA for Efficient Knockdown of the Target Gene. *ACS Omega* **2018**, *3*, 4871−4877.
(40) Senapati, S.; Sarkar, T.; Das, P.; Maiti, P. Layered Double Hydroxide Nanoparticles for Efficient Gene Delivery for Cancer Treatment. *Bioconjugate Chem.* **2019**, *30*, 2544−2554.
(41) Yoo, S. S.; Razzak, R.; Bédard, E.; Guo, L.; Shaw, A. R.; Moore, R. B.; Roa, W. H. Layered Gadolinium-Based Nanoparticle as a Novel Delivery Platform for MicroRNA Therapeutics. *Nanotechnology* **2014**, *25*, No. 425102.
(42) Yang, L.; He, X.; Jing, G.; Wang, H.; Niu, J.; Qian, Y.; Wang, S. Layered Double Hydroxide Nanoparticles with Osteogenic Effects as MiRNA Carriers to Synergistically Promote Osteogenesis of MSCs. *ACS Appl. Mater. Interfaces* **2021**, *13*, 48386−48402.
(43) Xu, Z. P.; Niebert, M.; Porazik, K.; Walker, T. L.; Cooper, H. M.; Middelberg, A. P. J.; Gray, P. P.; Bartlett, P. F.; Lu, G. Q. Subcellular Compartment Targeting of Layered Double Hydroxide Nanoparticles. *J. Controlled Release* **2008**, *130*, 86−94.
(44) Yu, Z.; Hu, P.; Xu, Y.; Bao, Q.; Ni, D.; Wei, C.; Shi, J. Efficient Gene Therapy of Pancreatic Cancer via a Peptide Nucleic Acid (PNA)-Loaded Layered Double Hydroxides (LDH) Nanoplatform. *Small* **2020**, *16*, 1907233.
(45) Tiwari, N.; Gheldof, A.; Tatari, M.; Christofori, G. EMT as the Ultimate Survival Mechanism of Cancer Cells. *Semin. Cancer Biol.* **2012**, *22*, 194−207.
(46) Kaufhold, S.; Bonavida, B. Central Role of Snail1 in the Regulation of EMT and Resistance in Cancer: A Target for Therapeutic Intervention. *J. Exp. Clin. Cancer Res.* **2014**, *33*, 62.
(47) Tang, X.; Sui, X.; Weng, L.; Liu, Y. SNAIL1: Linking Tumor Metastasis to Immune Evasion. *Front. Immunol.* **2021**, *12*, No. 724200.
(48) Kumarswamy, R.; Mudduluru, G.; Ceppi, P.; Muppala, S.; Kozlowski, M.; Niklinski, J.; Papotti, M.; Allgayer, H. MicroRNA-30a Inhibits Epithelial-to-Mesenchymal Transition by Targeting Snai1 and

https://doi.org/10.1021/acsomega.2c07866
ACS Omega 2023, 8, 18435−18448

Is Downregulated in Non-Small Cell Lung Cancer. *Int. J. Cancer* **2012**, *130*, 2044−2053.
(49) Singhai, R.; Patil, V.; Jaiswal, S.; Patil, S.; Patil, M. E-Cadherin as a Diagnostic Biomarker in Breast Cancer. *North. Am. J. Med. Sci.* **2011**, 227−233.
(50) Dong, H.; Xie, L.; Tang, C.; Chen, S.; Liu, Q.; Zhang, Q.; Zheng, W.; Zheng, Z.; Zhang, H. Snail1 Correlates with Patient Outcomes in E-Cadherin-Preserved Gastroesophageal Junction Adenocarcinoma. *Clin. Transl. Oncol.* **2014**, *16*, 783−791.
(51) Baranwal, S.; Alahari, S. K. Molecular Mechanisms Controlling E-Cadherin Expression in Breast Cancer. *Biochem. Biophys. Res. Commun.* **2009**, *384*, 6−11.
(52) Rosivatz, E.; Becker, K.-F.; Kremmer, E.; Schott, C.; Blechschmidt, K.; Höfler, H.; Sarbia, M. Expression and Nuclear Localization of Snail, an E-Cadherin Repressor, in Adenocarcinomas of the Upper Gastrointestinal Tract. *Virchows Arch.* **2006**, *448*, 277−287.
(53) Wang, X. Q.; Zhang, W.; Lui, E. L. H.; Zhu, Y.; Lu, P.; Yu, X.; Sun, J.; Yang, S.; Poon, R. T. P.; Fan, S. T. Notch1-Snail1-E-Cadherin Pathway in Metastatic Hepatocellular Carcinoma. *Int. J. Cancer* **2012**, *131*, E163−E172.
(54) Wang, W.; Shang, Y.; Li, Y.; Chen, S. Honokiol Inhibits Breast Cancer Cell Metastasis by Blocking EMT through Modulation of Snail/Slug Protein Translation. *Acta Pharmacol. Sin.* **2019**, *40*, 1219−1227.
(55) Farjadian, F.; Ghasemi, A.; Gohari, O.; Roointan, A.; Karimi, M.; Hamblin, M. R. Nanopharmaceuticals and Nanomedicines Currently on the Market: Challenges and Opportunities. *Nanomedicine* **2019**, *14*, 93−126.

https://doi.org/10.1021/acsomega.2c07866
ACS Omega 2023, 8, 18435−18448